ARCHIVIO ISTITUZIONALE
DELLA RICERCA

Alma Mater Studiorum Università di Bologna
Archivio istituzionale della ricerca

Chlorination and tautomerism: A computational and UPS/XPS study of 2-hydroxypyridine ⇌ 2-pyridone equilibrium

This is the final peer-reviewed author's accepted manuscript (postprint) of the following publication:

Published Version:
Chlorination and tautomerism: A computational and UPS/XPS study of 2-hydroxypyridine ⇌ 2-pyridone equilibrium / Melandri S.; Evangelisti L.; Canola S.; Sa'adeh H.; Calabrese C.; Coreno M.; Grazioli C.; Prince K.C.; Negri F.; Maris A.. - In: PHYSICAL CHEMISTRY CHEMICAL PHYSICS. - ISSN 1463-9076. - STAMPA. - 22:24(2020), pp. 13440-13455. [10.1039/d0cp02304c]

Availability:
This version is available at: https://hdl.handle.net/11585/781961 since: 2020-12-15

Published:

DOI: http://doi.org/10.1039/d0cp02304c

Terms of use:

Some rights reserved. The terms and conditions for the reuse of this version of the manuscript are specified in the publishing policy. For all terms of use and more information see the publisher's website.

This item was downloaded from IRIS Università di Bologna (https://cris.unibo.it/).
When citing, please refer to the published version.

(Article begins on next page)

03 May 2024

This is the final peer-reviewed accepted manuscript of:

Melandri, Sonia, Luca Evangelisti, Sofia Canola, Hanan Sa'adeh, Camilla Calabrese, Marcello Coreno, Cesare Grazioli, Kevin Charles Prince, Fabrizia Negri, and Assimo Maris. "Chlorination and tautomerism: a computational and UPS/XPS study of 2-hydroxypyridine≒ 2-pyridone equilibrium." Physical Chemistry Chemical Physics (2020).

The final published version is available online at:

https://doi.org/10.1039/D0CP02304C

© 2020

This version is subjected to the Royal Society of Chemistry terms for reuse that can be found at: https://www.rsc.org/journals-books-databases/librarians-information/products-prices/licensing-terms-and-conditions/#non-commercial-terms

Chlorination and tautomerism: a computational and UPS/XPS study of 2-hydroxypyridine ⇌ 2-pyridone equilibrium†

Sonia Melandri, [a] Luca Evangelisti, [a] Sofia Canola, [a] Hanan Sa'adeh, [b] Camilla Calabrese, [cd] Marcello Coreno, [e] Cesare Grazioli, [e] Kevin C. Prince, *[fg] Fabrizia Negri *[a] and Assimo Maris *[a]

The prototropic tautomeric equilibrium in 2-hydroxypyridine serves as a prototype model for the study of nucleobases' behaviour. The position of such an equilibrium in parent and chlorine monosubstituted 2-hydroxypyridine compounds in the gas phase was determined using synchrotron based techniques. The lactim tautomer is dominant for the 5- and 6-substituted compounds, whereas the parent, 3- and 4-substituted isomers have comparable populations for both tautomers. Information was obtained by measuring valence band and core level photoemission spectra at the chlorine L-edge and carbon, nitrogen, and oxygen K-edges. The effect of chlorine on the core ionization potentials of the atoms in the heterocycle was evaluated and reasonable agreement with a simple model was obtained. Basic considerations of resonance structures correctly predicts the tautomeric equilibrium for the 5- and 6-substituted compounds. The vibrationally resolved structure of the low energy portion of the valence band photoionization spectra is assigned based on quantum-chemical calculations of the neutral and charged species followed by simulation of the vibronic structure. It is shown that the first ionization occurs from a π orbital of similar shape for both tautomers. In addition, the highly distinctive vibronic structure observed just above the first ionization of the lactim, for three of the five species investigated, is assigned to the second ionization of the lactam.

Received 29th April 2020,
Accepted 28th May 2020

DOI: 10.1039/d0cp02304c

1 Introduction

Aromatic heterocycles play a key role in chemistry, biology, and pharmacology. Many of these compounds display the phenomenon of prototropic tautomerism, which is of great interest as it represents a model for intramolecular proton transfer and directly affects the reactivity and biochemical behavior of this class of compounds.[1]

For instance, nucleic acid bases have carbonyl and amino functional groups, which contain H-atoms that can take part in prototropic tautomerism:

$$\underset{\text{imino-enol}}{-\mathrm{N}=\mathrm{C(OH)}-} \rightleftharpoons \underset{\text{amino-keto}}{-\mathrm{NH}-\mathrm{CO}-}$$

Although the amino-keto forms (lactams) predominate under physiological conditions, it has been speculated that spontaneous formation of imino-enol tautomers (lactims) contribute to mutagenic mispairings during DNA replication, whereas in RNA, minor tautomeric forms have been proposed to enhance the structural and functional diversity of RNA enzymes and aptamers.[2] However, owing to the presence of more than two heteroatoms, the tautomeric equilibrium in nucleic acid bases is quite complicated. The study of simpler model molecules can be useful for understanding the behavior of these biological systems.

The 2-hydroxypyridine/2-pyridone pair (2HP/2PO, from now on) can be considered as a prototype system simulating the pyrimidine nucleic bases (cytosine, uracil, and thymine). The prototropic equilibrium of 2HP/2PO and related compounds strongly depends on the aggregation state and on the effects of substituents, and it has been the subject of extended experimental[3–13] and computational[14–17]

[a] Dipartimento di Chimica "G. Ciamician", Università di Bologna, via Selmi 2, I-40126 Bologna, Italy. E-mail: assimo.maris@unibo.it, fabrizia.negri@unibo.it
[b] Department of Physics, The University of Jordan, Amman, JO-11942, Jordan
[c] Departamento de Química Física, Facultad de Ciencia y Tecnología, Universidad del País Vasco (UPV/EHU), Apartado 644, E-48080 Bilbao, Spain
[d] Basque Centre for Biophysics (CSIC, UPV/EHU), Barrio Sarriena, E-48940 Leioa, Spain
[e] CNR-ISM, Trieste LD2 Unit, Elettra-Sincrotrone Trieste, I-34149 Basovizza, Trieste, Italy
[f] Elettra Sincrotrone Trieste, Area Science Park, I-34149 Basovizza, Trieste, Italy. E-mail: kevin.prince@elettra.eu
[g] Centre for Translational Atomaterials, Swinburne University of Technology, Melbourne, Australia

† Electronic supplementary information (ESI) available: Theoretical geometries, molecular orbitals and vibrational normal modes. See DOI: 10.1039/d0cp02304c

studies. The prediction of the equilibrium position in these systems turned out to be a difficult task for theoretical simulations: neither *ab initio* nor density functional theory (DFT) approaches, even using extended basis sets, provide reliable results. As a general rule of thumb, it was found that *ab initio* methods overestimate the stability of the lactim tautomer (2HP), whereas DFT methods overestimate the stability of the lactam form (2PO).

Experimental studies at low pressure in the gas phase are important because they provide information on the molecules without the interference of the surroundings, thus highlighting the intrinsic molecular behavior. Moreover, data acquired in isolated conditions can be directly compared to the theoretical results, allowing for a synergistic investigation method in which calculations drive the experimental assignment and experimental findings serve as benchmarks for calculations.

Photoemission spectroscopy constitutes an extremely useful tool for both the determination of the concentration of molecular species and for studying the electronic structure of molecules. For instance, core level spectroscopy showed that, in the gas phase, uracil exists in the lactam form only whereas cytosine exists in both tautomeric forms, with the lactim one being more stable.[18]

In a recent report, the tautomeric and conformational equilibria of 2HP/2PO have been explored by studying the role of chlorination at different ring positions and the influence of the solvent.[19] Combining rotational spectroscopy experiments and quantum mechanical calculations, a semi-empirical model for the estimation of the relative stability of the tautomers was proposed: it was found that theoretical shifts due to chlorination can be combined with the experimental relative energies of the unsubstituted species to achieve reliable predictions.

In this paper we present a comparative study of the gas phase valence band and core level photoemission spectra of 2HP/2PO and its four mono-chlorinated analogues:

- 3-Cl-2-hydroxypyridine/3-Cl-2-pyridone (3Cl-2HP/3Cl-2PO)
- 4-Cl-2-hydroxypyridine/4-Cl-2-pyridone (4Cl-2HP/4Cl-2PO)
- 5-Cl-2-hydroxypyridine/5-Cl-2-pyridone (5Cl-2HP/5Cl-2PO)
- 6-Cl-2-hydroxypyridine/6-Cl-2-pyridone (6Cl-2HP/6Cl-2PO)

The primary aim of this study is to determine the relative stability of the tautomers (thus verifying the reliability of the semi-empirical model proposed by Calabrese *et al.*[9]) and understand the factors which determine the tautomeric equilibrium in the ground state S_0 of the neutral species. Moreover, by complementing the spectral analysis with computational investigations, we also acquire information on the cationic forms of the investigated species. In particular, the rich vibronic structure observed in the low energy region of the valence band photoemission spectra, is assigned to the ionization of lactam and lactim forms in their ground D_0 and lowest excited D_1 cationic states, based on quantum-chemical calculations supplemented by the simulation of vibronic structures.

2 Experimental methods

Photoemission spectra of 2HP/2PO and its four mono-chlorinated analogues were recorded at the gas phase beamline[20] at the Elettra synchrotron light source (Trieste, Italy) using an electron energy analyser described previously.[21] All compounds are solid powders at room temperature. They were purchased from Alfa Aesar (purity 98% for all compounds except 5Cl-2HP/5Cl-2PO, with 97% purity) and introduced into the experimental chamber without further purification. The samples were sublimated using a custom-built, resistively heated furnace, based on a stainless steel crucible, a Thermocoax® heating element, and a type K thermocouple. The temperature was increased until a pressure of about $p = 0.5 \pm 0.2$ mPa was reached.

Table 1 Experimental setup parameters

Spectral region	Photon en. [eV]	Resolution [eV]	Calibrant	Binding en. [eV]
Valence	97	0.055	$Ar(3p_{3/2})$	15.76[23]
C(1s)	392	0.140	C(1s), CO_2	297.70[24]
O(1s)	628	0.320	O(1s), CO_2	541.08[25]
N(1s)	495	0.220	N(1s), N_2	409.50[25]
Cl(2p)	275	0.130	$S(2p_{3/2})$, SF_6	180.21[25]

The X-ray Photoemission Spectroscopy (XPS) and the valence Photoemission Spectroscopy (PES) data were recorded using a VG-Scienta SES-200 photoelectron analyzer[22] mounted at magic angle (54.7°). The use of this angle allows us to record spectra in which the intensities of all peaks is proportional to the angle-integrated intensity, that is, angular effects are eliminated. The valence and core spectra were taken using the photon energies, resolution and calibrants given in Table 1. The photon energies were chosen to be about 100 eV above threshold in order to avoid the effects of post-collision interaction.

3 Computational methods

To support the assignment of the experimental spectral features, the adiabatic ionization potentials were calculated using the Gaussian16™‡ software package (G16, Rev. A.03).

Core–shell ionization potentials were computed by means of the Symmetry Adapted Cluster/Configuration Interaction method (SAC-CI[26]) implemented in G16 with the cc-pVTZ basis set, on the structures optimized at the MP2/aug-cc-pVTZ level.

As regards the prediction of the outer valence band behaviour, a DFT approach was used. The photoionization potentials were obtained as the difference between the energy of the molecules in the neutral ground state (S_0) and the molecules in the cationic ground state (D_0) and cationic excited state (D_1). For S_0 and D_0, geometry optimization and harmonic vibrational frequency calculations were run at the B3LYP/aug-cc-pVTZ level, whereas time-dependent (TD)-B3LYP/aug-cc-pVTZ was used for D_1.

The vibronic structure associated with each ionization in the low energy region of the photoelectron spectra was simulated including the Franck–Condon activities[27] determined by the evaluation of the Huang–Rhys factors S_k[28] for each vibrational mode k with frequency ν_k. S_k was obtained using the equation:

$$S_k = \frac{1}{2} \cdot B_k^2 \qquad (1)$$

‡ Gaussian is a registered trademark of Gaussian, Inc. 340 Quinnipiac St. Bldg. 40 Wallingford, CT 06492 USA.

where B_k is the dimensionless displacement parameter defined, assuming the harmonic approximation, and neglecting Duschinsky[29] rotation, as:

$$B_k = \left(\frac{2\pi\nu_k}{\hbar}\right)^{1/2} \cdot (X_j - X_i) \cdot M^{1/2} \cdot Q_k(j) \qquad (2)$$

where X_i (or X_j) is the $3N$ dimensional vector of the equilibrium Cartesian coordinates of the i (or j) electronic state (here i is the neutral and j is the cationic state), M is the $3N \times 3N$ diagonal matrix of atomic masses and $Q_k(j)$ is the $3N$ dimensional vector describing the kth normal coordinate of the j (cationic) state in terms of mass weighted Cartesian coordinates. While the approach is less rigorous than that discussed in recent work,[30–32] it is justified by the minor changes computed for the active vibrational modes upon ionization. For each normal mode k, the Franck–Condon factor FC for a transition from a vibrational level m (of the neutral molecule) to the vibrational level n (of the cation) is:[28]

$$\mathrm{FC}_k(m,n)^2 = \mathrm{e}^{-S_k} \cdot S_k^{n-m} \cdot \frac{m!}{n!} \cdot \left[L_m^{n-m}(S_k)\right]^2 \qquad (3)$$

where L is a Laguerre polynomial. The intensity $I_k(m,n)$ of the m to n transition for the normal mode k is given by the FC factor, weighted for the population of the m vibrational state:

$$I_k(m,n) = \mathrm{FC}_k(m,n)^2 \cdot \frac{1}{Z} \cdot \exp\left(-\frac{m\hbar\omega_k}{k_\mathrm{B}T}\right) \qquad (4)$$

with k_B the Boltzmann constant, T the temperature and Z the partition function. The total intensity of the multimode vibrational transition, including all the active normal modes, is the simple product of the monodimensional intensities.[28] Photoelectron spectra were simulated at T = 0 K and a Gaussian broadening function (full width at half maximum FWHM = 0.06 eV) was convoluted with each computed intensity.

4 Results and discussion

The tautomeric conversion between 2HP (lactim) and 2PO (lactam) is represented in Fig. 1. The molecular system is characterized by three conjugated π bonds. Because of resonance zwitterionic structures (also shown in Fig. 1) they are delocalized on all the heavy atoms, thus both tautomers are planar. The planarity is maintained also when substituting a hydrogen atom in position 3, 4, 5 or 6 with a chlorine atom.

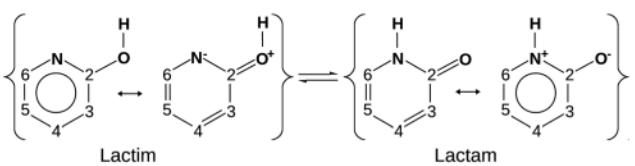

Fig. 1 Tautomeric equilibrium between 2-hydroxypyridine and 2-pyridone (neutral and zwitterionic forms) and numbering of the atoms used in the text.

4.1 Oxygen (1s) and nitrogen (1s) ionization

The photoionization spectra at the O(1s) and N(1s) edges are reported in Fig. 2 and 3, respectively. It is immediately evident from the spectra that at least two tautomers are present in some of these compounds. The nitrogen and oxygen spectra clearly show two peaks in the spectra of parent, 3-Cl and 4-Cl species, although only one of each of these atoms is present in each molecule. Our calculations assign the O(1s) peaks with higher ionization potential (IP) to hydroxyl oxygen (lactim form), and the peaks with lower IP to carbonyl oxygen (lactam form). Similarly, the higher binding energy N(1s) peaks are assigned to an amino species (lactam form), and the lower ones to imino nitrogen (lactim form). This assignment is consistent with previous XPS reports on 2HP/2PO[4] and nucleobases.[18] However, also in 5-Cl and 6-Cl species a second weak peak was detected, as seen in the enlarged spectra reported in Fig. 2 and 3. At a qualitative level, since the signal intensities reflect the abundances of the tautomers, we conclude that 6-Cl species is present almost completely as the lactim form, 5-Cl species has a low population of the lactam form, while the other compounds have comparable populations of both lactam and lactim tautomers. From the peak intensity ratios, we calculate the ratio of populations of the tautomers in Section 4.4. The experimental peak values are compared to the SAC-CI[26] theoretical vertical IPs in Table 2. The computations overestimate the IP values by about 1 eV, and the discrepancies are larger for lactam forms, namely: 0.8–0.9 eV for hydroxyl O(1s), 1.1–1.2 eV for carbonyl O(1s), 1.1–1.2 eV for imino N(1s), and 1.3–1.4 eV for amino N(1s).

4.2 Carbon (1s) ionization

The presence of two tautomers in the gaseous mixture is also evident in the C(1s) spectra (Fig. 4–8) although the interpretation is less straightforward. The parent and 3-Cl compounds display 6 peaks, whereas only 5 are expected from the stoichiometry of a single tautomer. 4-Cl species displays 5 peaks, but the ratio of intensities is far from stoichiometric. As noted above, the N(1s) and O(1s) spectra have established that for 5-Cl and 6-Cl species the dominant tautomer is the lactim form and the population of lactam is very small or negligible. This is consistent with the C(1s) spectra of 5Cl-2HP and 6Cl-2HP, which show five nearly stoichiometric peaks, corresponding to the 5 core states expected.

Comparing with the theoretical data (Table 2) and assuming that the most intense peaks in the spectra of the other compounds (2HP/2PO, 3Cl-2HP/3Cl-2PO and 4Cl-2HP/4Cl-2PO) belong to the lactim tautomer, a general trend can be deduced: the carbon atom bound to the oxygen atom (the most electronegative), C2, corresponds to the highest binding energy peak (IP = 293.1–293.4 eV). Then in order of decreasing binding energy value one finds the carbon atom bound to the chlorine atom (IP = 291.6–292.9 eV), the carbon atom bound to the nitrogen atom, C6 (IP = 291.4–291.9 eV), then C4 (IP = 291.0–291.2 eV), and finally, with similar binding energy, C3 and C5 (IP = 290.3–290 eV). The resulting assignment is reported in Fig. 4–8.

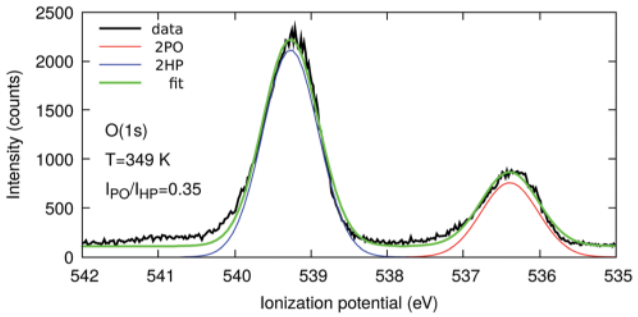

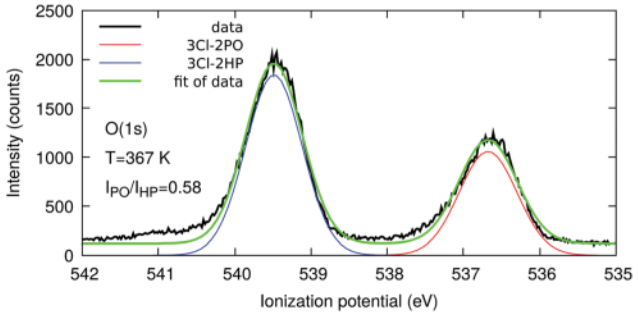

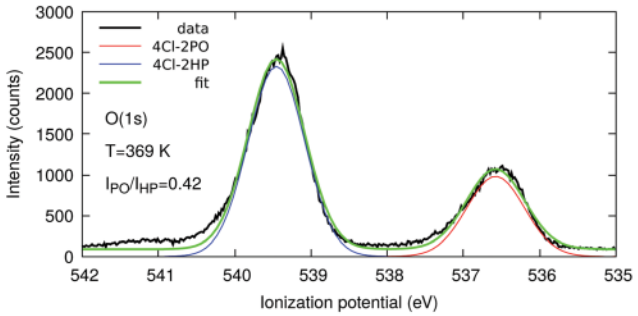

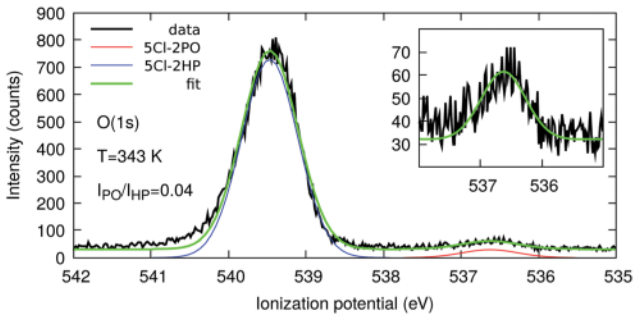

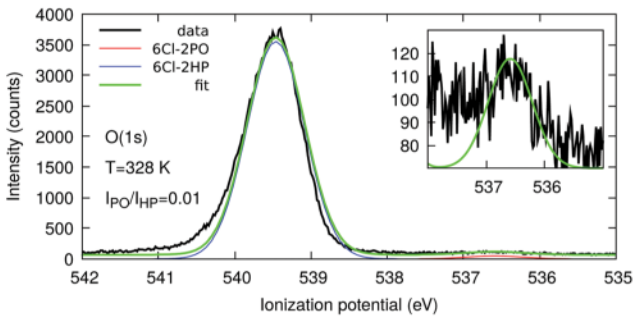

Fig. 2 Experimental and fitted photoemission spectra of parent and chlorinated 2-hydroxypyridine and 2-pyridone at the O(1s) edge.

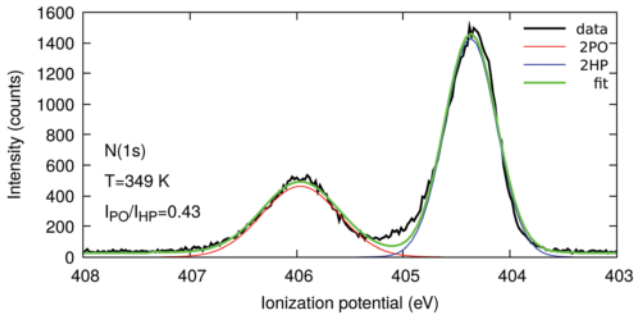

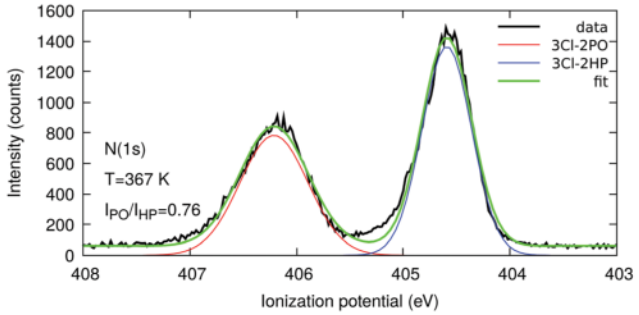

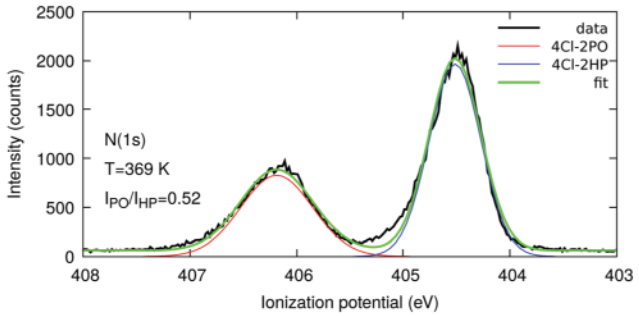

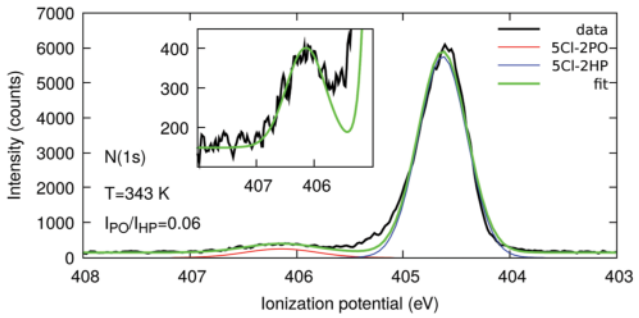

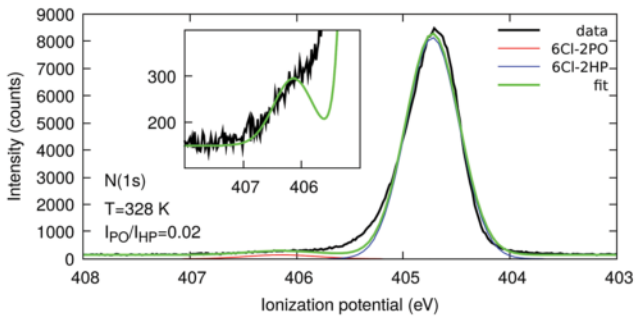

Fig. 3 Experimental and fitted photoemission spectra of parent and chlorinated 2-hydroxypyridine and 2-pyridone at the N(1s) edge.

Table 2 Observed and calculated (SAC-CI/cc-pVTZ//MP2/aug-cc-pVTZ) inner shell ionization potentials, in eV, for parent and chlorinated 2-hydroxypyridine and 2-pyridone compounds. Shift of the ionization potential due to chlorination referred to the parent compound are given in parentheses

	Lactim (imino-enol)			Lactam (amino-keto)		
O(1s)	Obs.	Calc.	c.–o.	Obs.	Calc.	c.–o.
Parent	539.27	540.100	0.83	536.40	537.540	1.14
3-Cl	539.49 (0.22)	540.296 (0.20)	0.81	536.68 (0.28)	537.798 (0.26)	1.12
4-Cl	539.45 (0.18)	540.336 (0.24)	0.89	536.58 (0.18)	537.760 (0.22)	1.18
5-Cl	539.47 (0.20)	540.268 (0.17)	0.80	536.62 (0.22)	537.819 (0.28)	1.20
6-Cl	539.46 (0.19)	540.339 (0.24)	0.88	536.59 (0.19)	537.737 (0.20)	1.15
	Lactim (imino-enol)			Lactam (amino-keto)		
N(1s)	Obs.	Calc.	c.–o.	Obs.	Calc.	c.–o.
Parent	404.37	405.552	1.18	405.96	407.290	1.33
3-Cl *meta*[a]	404.59 (0.22)	405.752 (0.20)	1.16	406.21 (0.25)	407.520 (0.23)	1.31
4-Cl *para*	404.51 (0.14)	405.706 (0.15)	1.20	406.19 (0.23)	407.497 (0.21)	1.31
5-Cl *meta*'	404.63 (0.26)	405.801 (0.25)	1.17	406.14 (0.18)	407.510 (0.22)	1.37
6-Cl *ortho*	404.73 (0.36)	405.857 (0.31)	1.13	406.14 (0.18)	407.498 (0.21)	1.36
	Lactim (imino-enol)			Lactam (amino-keto)		
C(1s) parent	Obs.	Calc.	c.–o.	Obs.	Calc.	c.–o.
C2(1s)	293.08	293.871	0.79	293.52	294.466	0.95
C3(1s)	290.59	291.144	0.55	290.44	291.104	0.66
C4(1s)	291.01	291.830	0.82	291.27	292.061	0.79
C5(1s)	290.30	291.042	0.74	290.80	291.271	0.47
C6(1s)	291.44	292.274	0.83	291.92	293.095	1.18
$\langle$C(1s)$\rangle$[b]	291.28	292.03	0.75	291.59	292.399	0.81
	Lactim (imino-enol)			Lactam (amino-keto)		
C(1s) 3-Cl	Obs.	Calc.	c.–o.	Obs.	Calc.	c.–o.
C2(1s) *ortho*	293.31 (0.23)	294.156 (0.29)	0.85	293.83 (0.31)	294.760 (0.29)	0.93
C3(1s) *ipso*	291.97 (1.38)	292.528 (1.38)	0.56	291.52 (1.08)	292.477 (1.37)	0.96
C4(1s) *ortho*'	291.13 (0.12)	292.011 (0.18)	0.88	291.36 (0.09)	292.184 (0.12)	0.82
C5(1s) *meta*'	290.65 (0.35)	291.318 (0.28)	0.67	290.90 (0.10)	291.503 (0.23)	0.60
C6(1s) *para*	291.78 (0.34)	292.426 (0.15)	0.65	292.13 (0.21)	293.227 (0.13)	1.10
$\langle$C(1s)$\rangle$	291.77	291.49	0.72	291.95	292.83	0.88
	Lactim (imino-enol)			Lactam (amino-keto)		
C(1s) 4-Cl	Obs.	Calc.	c.–o.	Obs.	Calc.	c.–o.
C2(1s) *meta*	293.34 (0.26)	294.196 (0.33)	0.86	293.78 (0.26)	294.741 (0.27)	0.96
C3(1s) *ortho*	290.70 (0.11)	291.374 (0.23)	0.67	290.81 (0.37)	291.290 (0.19)	0.48
C4(1s) *ipso*	292.43 (1.42)	293.256 (1.43)	0.83	292.46 (1.19)	293.453 (1.39)	0.99
C5(1s) *ortho*'	290.62 (0.32)	291.292 (0.25)	0.67	291.00 (0.20)	291.524 (0.25)	0.52
C6(1s) *meta*'	291.64 (0.20)	292.610 (0.34)	0.97	292.31 (0.39)	293.428 (0.33)	1.12
$\langle$C(1s)$\rangle$	291.75	292.55	0.80	292.07	292.89	0.82

The five carbon atoms present in each of the two tautomers give rise to 10 core level ionic states with significant intensity for 2HP/2PO, 3Cl-2HP/3Cl-2PO and 4Cl-2HP/4Cl-2PO. At first it may seem that little quantitative information can be extracted from such complex spectra, but we found that a considerable amount of information can be obtained, because the spectra are rather highly constrained and cannot be fitted simply by 10 independent peaks. As noted above, theory indicates that the peaks at about 293.1–293.4 eV, in all compounds, belong to carbon bonded to a hydroxyl group. Theory also indicates that signals of carbon in a carbonyl group are expected to lie at higher IP values. This allows a determination of the population ratio in each isomer, in addition to that provided by the oxygen and nitrogen core levels. Secondly, the intensities of the other four carbon atoms in the two tautomers should follow the population ratio to a good approximation. Thirdly, the widths of the peaks (determined by Franck–Condon factors and hole lifetime) are known to fall in a restricted range, for example, they are not narrower than the core hole lifetime.

We applied all of these constraints in a routine to fit the experimental spectra. The initial guesses for the IPs were the theoretical IPs. The intensity ratio between tautomers was kept constant but for a given tautomer, small variations of intensity between ionic states were allowed. The constraints on IPs and width were gradually relaxed at each cycle of fitting, with the IPs allowed to vary by small increments. Using this procedure, we were able to decompose the measured spectra into the spectra of the individual tautomers, and compare the IPs with theory.

Table 2 *(continued)*

	Lactim (imino-enol)			Lactam (amino-keto)
C(1s) 5-Cl	Obs.	Calc.	c.–o.	Calc.
C2(1s) *para*	293.39 (0.31)	294.103 (0.23)	0.71	294.730 (0.26)
C3(1s) *meta*	290.80 (0.21)	291.470 (0.33)	0.67	291.461 (0.36)
C4(1s) *ortho*	291.20 (0.19)	292.111 (0.28)	0.91	292.340 (0.28)
C5(1s) *ipso*	291.64 (1.34)	292.458 (1.42)	0.82	292.655 (1.39)
C6(1s) *ortho′*	291.90 (0.46)	292.556 (0.28)	0.66	293.328 (0.23)
⟨C(1s)⟩	291.79	291.54	0.75	292.90
	Lactim (imino-enol)			Lactam (amino-keto)
C(1s) 6-Cl	Obs.	Calc.	c.–o.	Calc.
C2(1s) *meta*	293.41 (0.33)	294.231 (0.36)	0.82	294.725 (0.28)
C3(1s) *para*	290.86 (0.27)	291.314 (0.17)	0.45	291.242 (0.14)
C4(1s) *meta′*	291.19 (0.18)	292.134 (0.30)	0.94	292.184 (0.12)
C5(1s) *ortho′*	290.67 (0.37)	291.310 (0.27)	0.64	291.467 (0.20)
C6(1s) *ipso*	292.88 (1.44)	293.746 (1.47)	0.87	294.448 (1.35)
⟨C(1s)⟩	291.80	292.55	0.74	292.83
	Lactim (imino-enol)			Lactam (amino-keto)
Cl(2p)	Obs. ($2p_{1/2}$; $2p_{3/2}$)	Calc. ($2p_{x/y/z}$)	c.–o.	Calc. ($2p_{x/y/z}$)
3-Cl	207.93; 206.32	207.485/.580/.506	0.67	207.327/.427/.349
4-Cl	208.16; 206.55	207.820/.917/.842	0.77	207.887/.982/.909
5-Cl	208.02; 206.40	207.590/.682/.607	0.69	207.823/.918/.843
6-Cl	207.85; 206.23	207.542/.635/.563	0.81	208.490/.586/.508

[a] Position with respect the Cl substituent. [b] Value averaged on all carbon atoms.

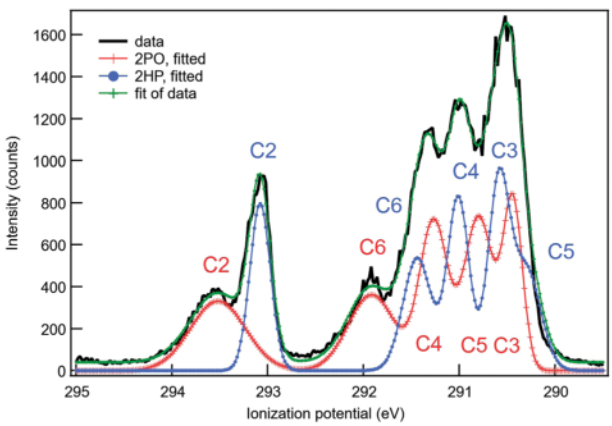

Fig. 4 Experimental and fitted photoemission spectra of 2HP/2PO at the C(1s) edge.

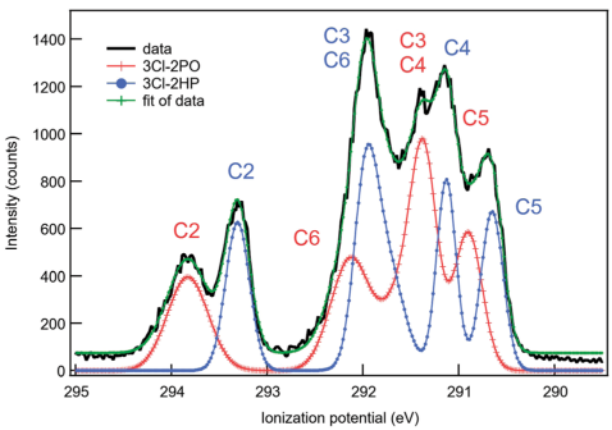

Fig. 5 Experimental and fitted photoemission spectra of 3Cl-2HP/3Cl-2PO at the C(1s) edge.

The carbon 1s spectra are shown in Fig. 4–8 together with theoretical curves, and the respective IPs obtained by fitting, are given in Table 2. As well as the fitted experimental and calculated IPs, the root mean square differences between these quantities are given. It is clear that this procedure does not give the absolute best fit of the data, but rather a plausible interpretation which is a minimum in the available parameter space.

For the lactim forms of the compounds, the root mean square differences between theory and experiment are: 0.76 eV (2HP), 0.73 eV (3Cl-2HP), 0.81 (4Cl-2HP), 0.76 eV (5Cl-2HP) and 0.77 eV (6Cl-2HP). For the lactam forms the deviations from the theoretical values are: 0.84 eV (2PO), 0.90 eV (3Cl-2PO) and 0.86 eV (4Cl-2PO). There are no experimental C(1s) data for 5Cl-2PO and 6Cl-2PO as the populations were too small to give an adequate signal. As found for O(1s) and N(1s) peaks, the deviations for lactams are 0.1–0.2 eV larger than those of lactims, indicating acceptable agreement. Overall we conclude that the theoretical and fitted experimental spectra are consistent. Because several approximations are made during the fitting procedure, such as the assumption of symmetric peaks, we believe that the observed discrepancies between theory and experiment may arise mostly from the fitting.

4.3 Chlorine (2p) ionization

The Cl(2p) spectra consist of a $2p_{3/2,1/2}$ doublet (Fig. 9). In line with the spin multiplicity, the intensity ratio of the peaks is

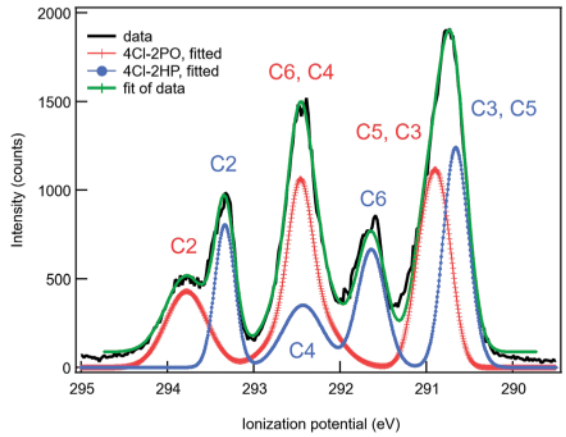

Fig. 6 Experimental and fitted photoemission spectra of 4Cl-2HP/4Cl-2PO at the C(1s) edge.

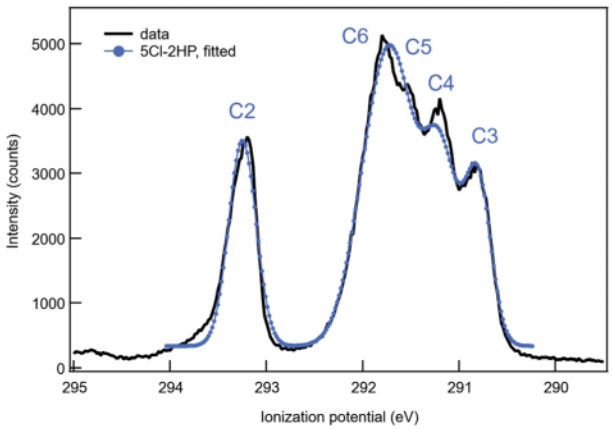

Fig. 7 Experimental and fitted photoemission spectra of 5Cl-2HP at the C(1s) edge.

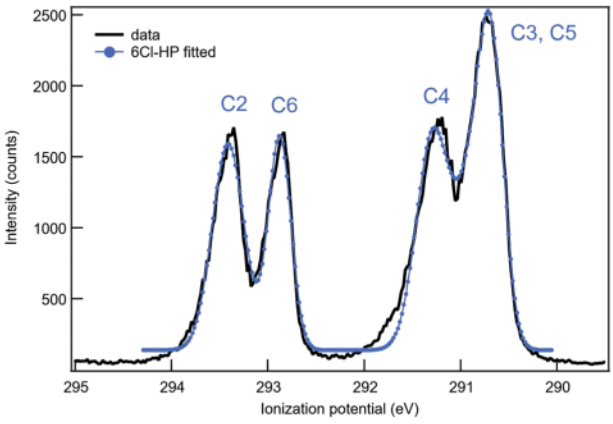

Fig. 8 Experimental and fitted photoemission spectra of 6Cl-2HP at the C(1s) edge.

$I(2p_{1/2}) : I(2p_{3/2}) = 1 : 2$. The experimental spin-orbital splitting is 1.61 eV for 3Cl-2HP and 4Cl-2HP, and 1.62 eV, for 5Cl-2HP and 6Cl-2HP, which is within the error of the measurement.

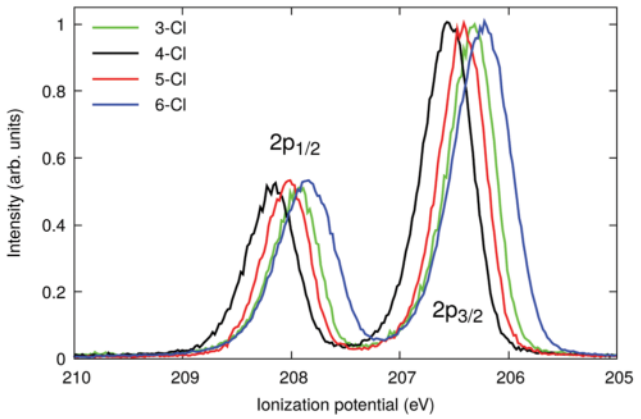

Fig. 9 Photoemission spectra of chlorinated 2-hydroxypyridine and 2-pyridone at the Cl(2p) edge.

The computed IPs for $2p_x$, $2p_y$ and $2p_z$ are quite close to each other (within about 0.1 eV, Table 2), and, as a consequence, the corresponding peaks are not resolved. In other words the molecular field splitting is weak. Also the shift between the tautomers for 3-Cl and 4-Cl species are predicted to be about 0.1 eV. This agrees with the spectra where no additional peaks are observed. As regards 5-Cl and 6-Cl species, the expected shifts are larger (−0.24 and 0.95 eV, respectively), but due to the low lactam abundance, no signals were observed. As found for C(1s), N(1s) and O(1s), SAC-CI/cc-pVTZ calculations overestimate the IP values; for Cl(2p) the difference with respect the weighted average of the observed peaks is 0.7–0.8 eV.

The four Cl(2p) spectra show small shifts as a function of the position of the Cl atom in the isomer. The 4-Cl species, in which the Cl atom is located farthest from the O and N atoms, has the highest ionization potential, followed by the 5-Cl, 3-Cl and 6-Cl isomers. This approximately reflects the distance from the heteroatoms, and the shifts in ionization potential are largely determined by screening effects of the final state. The further the chlorine atom is from the electronegative heteroatoms, the easier it is to attract charge to the final ionic state.

4.4 The tautomeric equilibrium in S_0 the state

All 1s core level spectra show effects due to isomerism, but the most direct information is obtained from the N(1s) and O(1s) spectra. This is because the imino/amino and carbonyl/hydroxyl peaks are well separated in ionization potential and so their relative integrated intensities can be easily determined. Since XPS is to a good approximation quantitative, the N and O core level spectra therefore provide independent estimates of the relative populations of the lactam and lactim tautomers. The results are shown in Table 3.

We note a discrepancy in Table 3 between the population ratios derived from the O(1s) and N(1s) core level intensities. This is assigned to small differences in the pole strengths for ionization of the core levels. It is well-known that atoms in conjugated bonds tend to have stronger satellite structure, and therefore reduced pole strength for the main line. For oxygen, the ratio of intensities is between carbonyl oxygen and

Table 3 Estimated lactam to lactim populations from the ratios of C2(1s), N(1s) and O(1s) ionization signals, selected relative abundances (RA = N_{lactam}/N_{lactim}), experimental working temperature and relative energy of the tautomers ($\Delta E = E_{lactam} - E_{lactim}$)

	Parent	3-Cl	4-Cl	5-Cl	6-Cl
C2(1s)	0.77	0.93	0.77	—	—
N(1s)	0.43	0.76	0.52	0.04	0.01
O(1s)	0.35	0.58	0.42	0.06	0.02
RA	0.39	0.69	0.47	0.05	0.015
T (K)	349	367	369	343	328
ΔE (kJ mol^{-1})	2.7	1.1	2.3	8.5	11.5
	2.4(3)[a]	1.4[b]	2.4[b]	10.4[b]	13.5[b]
	3.2(4)[c]	2.2[d]	2.6[d]	10.3[d]	15.4[d]

[a] XPS data.[4] [b] Semiempirical values derived from MP2/aug-cc-pVTZ calculations.[19] [c] Rotational spectroscopy data.[6] [d] Semiempirical values derived from B3LYP/aug-cc-pVTZ calculations.[19]

hydroxy oxygen, so the numerator is reduced. For nitrogen, the situation is reversed as the ratio is between amino nitrogen and imino nitrogen, thus the denominator is reduced. This interpretation is consistent with the fact that the ratios for nitrogen are all about 20% higher than those of oxygen. We conclude that the best estimate of the populations is given by the mean of the values for N and O, with an estimated error of 10%, RA in Table 3.

This effect appears to be even stronger for the C2 carbon atom, whose local chemical environment changes from N–C═O to N═C–OH between the two tautomers. The C2 intensity ratio qualitatively follows that of O and N, but not quantitatively, so we conclude the C2 intensity ratio is a less accurate measure of tautomer population. Such a large discrepancy is generally exceptional, but some cases are known, for example in benzaldehyde, as much as 50% of the O(1s) pole strength appears as satellite structure.[33]

The relative energy values derived from the selected relative abundances are given in Table 3, and compared with experimental[4,6] (2HP/2PO) and semiempirical[19] (3Cl-2HP/3Cl-2PO, 4Cl-2HP/4Cl-2PO, 5Cl-2HP/5Cl-2PO, 6Cl-2HP/6Cl-2PO) relative energies.

4.5 Effect of chlorine on the tautomeric equilibrium in the S_0 state

Thomas *et al.*[34,35] considered the carbon core level ionization potentials in di-substituted benzene molecules, focusing on the energy shifts induced by the substituents. In the simplest version of their model, they approximated the ionization potential of each C(1s) level of the di-substituted molecule by the sum of the ionization potential shifts for each substituent separately, with respect to the parent compound (benzene). They labelled the atoms as *ipso* (to which the substituent was bonded), *ortho*, *meta* and *para*. By symmetry, for a single substituent attached to a benzene molecule, only these four shifts occur. The nitrogen atom in the pyridine ring of the present samples breaks the symmetry of the *ortho* and *meta* positions, so we refer to these atoms as *meta* and *ortho* when the carbon atom is on the side of the molecule containing oxygen (C2, C3, C4) and *meta′* and *ortho′* when the carbon atoms are closer to the nitrogen atom (C4, C5, C6) (Fig. 10).

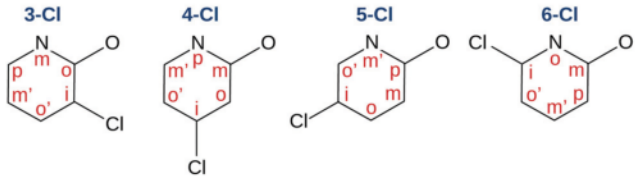

Fig. 10 Labeling of the ring atoms with respect to the position of chlorine atom (*i* = *ipso*, *o* = *ortho*, *m* = *meta*, *p* = *para*) chlorinated analogues of 2-hydroxypyridine and 2-pyridone.

Their discussion concerned only carbon atoms, but we can generalise the discussion and consider the IPs of the nitrogen atoms in the present compounds, using the same nomenclature for the position of the chlorine atoms. We compare in Table 2 the energy shifts of the IP due to chlorination, referred to the parent compound. It is evident that the energy shifts of N(1s) are similar for Cl in the *meta* (3Cl-2HP) and *meta′* (5Cl-2HP) positions, with values of 0.24 ± 0.02 eV (experimental), or 0.225 ± 0.025 eV (theory). The shift related to Cl in the *para* position (4Cl-2HP), is significantly smaller (0.14 eV), while the shift due to Cl at the *ortho* (6Cl-2HP) position is substantially larger, 0.36/0.31 eV (experiment/theory). Although these shifts are relatively small, the result suggests that within a classical model of resonance *versus* induction, the induction effect (charge withdrawal) dominates.

In other words, the shift of N(1s) due to the presence of the electron withdrawing Cl depends principally on the distance between nitrogen and the Cl atom. Resonance effects appear to be less important, presumably because the Cl lone pairs have limited overlap with the delocalised orbitals of the pyridine ring. The situation is different for the lactam tautomer, where the N(1s) shifts are nearly independent (0.18–0.25 eV) of the position of the Cl atom. In this case, the nitrogen π orbitals polarised perpendicular to the plane of the ring have limited hybridisation with delocalised orbitals, while the carbonyl π orbital may hybridise. However it appears that the charge withdrawal and resonance effects combine to cancel any effect related to the position of the Cl atom. For O(1s), the experimental shifts due to chlorination cover a slightly greater range in lactam tautomers (0.18–0.28 eV) than in lactim tautomers (0.18–0.22 eV).

We now consider the zwitterionic resonance structures of the two tautomers (Fig. 1) and the possible stabilizing effect of a chlorine electron-withdrawing substituent. In the case of lactims there is a negative charge on the nitrogen atom, while in lactams there is a negative charge on the oxygen atom. A chlorine atom near the nitrogen (position 5 and 6) or oxygen (position 3) should then stabilize the lactim or the lactam tautomer, respectively. This is indeed observed: 5Cl-2HP and 6Cl-2HP are by far the most abundant tautomers, while 3Cl-2HP/3Cl-2PO is the species showing the highest N_{lactam}/N_{lactim} ratio. Correspondingly, the larger shifts of IPs are those of N(1s) in 6Cl-2HP (0.36 eV) and O(1s) in 3Cl-2PO (0.28 eV). As regards 4Cl-2HP/4Cl-2PO, the same number of bonds separates Cl from both N and O, and actually the N_{lactam}/N_{lactim} ratio is close to that of the parent species.

Among carbon atoms, those to which Cl is bonded (*ipso* position), show the larger IP shifts: 1.34–1.44 eV for lactims, similar to the 1.4 eV value observed upon chlorination of benzene,[36] and 1.08–1.19 eV for lactams, in good agreement with the 1.12 eV shift observed for the uracil/5-chloro-uracil pair.[18,37] All the predicted values lie in the 1.35–1.47 eV range, reproducing correctly the lactim values and overestimating the lactam ones. The experimental IP shifts for carbon atoms in the *para* position is greater by about 0.3 eV for 3Cl-2HP, 5Cl-2HP and 6Cl-2HP and it is 0.21 eV for 3Cl-2PO. In all cases the computed values underestimate the shift by 0.1–0.2 eV. For the remaining carbon atoms, the IP shifts are in the range 0.11–0.46 eV (experimental) or 0.18–0.36 eV (theory) for lactims and 0.09-0.39 eV (experimental) or 0.12–0.36 eV (theory) for lactams.

4.6 Valence band photoionization spectrum

It is well known that photoelectron spectroscopy in the valence band region represents one of the most direct probes of the bonding properties of molecules and a test for electronic structure theories through the identification of molecular orbitals. In particular, the vibronic structure associated with a specific ionization channel provides information on the nature of the molecular orbital from which the electron has been ejected.

In this section we investigate the vibronic structure of the low energy portion of the photoelectron spectra. Due to the presence of both tautomers with similar populations in the neutral ground state (for most of the systems investigated), the spectra show a particularly rich and complex sequence of bands. The spectra measured in the 8–11 eV binding energy region, are shown in Fig. 11 (2HP/2PO, 3Cl-2HP/3Cl-2PO and 4Cl-2HP/4Cl-2PO), 12 (5Cl-2HP/5Cl-2PO) and 13 (6Cl-2HP/6Cl-2PO).

In the case of the parent compound 2HP/2PO, the vibronic fine structure has been reported previously by Poully *et al.*[10] using a cold molecular beam and an analyser with resolution down to 9 meV (73 cm^{-1}). They assigned the peaks lying at 8.443 and 8.933 eV to the $\tilde{X}0_0^0$ transition between the neutral and cation forms of 2PO and 2HP, respectively. In addition they tentatively assigned the origin of the $\tilde{X} \rightarrow \tilde{A}$ ($S_0 \rightarrow D_1$) transition of 2PO to the band observed at 9.54 eV, and the strong band at 9.372 to the $\tilde{X}1_0^1$ vibronic band of the $\tilde{X} \rightarrow \tilde{X}$ ($S_0 \rightarrow D_0$) transition, involving the hydroxyl stretching mode of 2HP.

The experimental data reported here for the parent molecule and the chlorinated derivatives shows that similar features appear systematically in some spectra and are missing in others. This is the case for the sequence of sharp bands observed in the region around 9.5 eV for the parent compound, and at slightly higher energies for 3-Cl and 4-Cl substituted species, which are missing in the spectra of 5-Cl and 6-Cl substituted species. Based on the relative population of tautomers discussed in Section 4.4 we know that the population of the 2HP tautomer is always larger in the ground state of the neutral species and is by far dominant for 5-Cl and 6-Cl substituted species. Because these are the only two species whose spectra do not show the sequence of three to four sharp bands in the region around 9.5 eV, we conclude that these distinctive signals must be attributed to the lactam tautomer and in Section 4.10 we show that the simulated vibronic structures entirely support this assignment. Apart from this apparent simplification in the photoemission spectra of 5-Cl and 6-Cl substituted species, the rich structure in the 8–11 eV region is difficult to disentangle for all five spectra reported here and calls for computational support.

For each tautomer we model not only the vibronic structure of the $S_0 \rightarrow D_0$ ($\tilde{X} \rightarrow \tilde{X}$) transition but also that of the second group of bands ($S_0 \rightarrow D_1$ or $\tilde{X} \rightarrow \tilde{A}$), using DFT and TD-DFT calculations for generating the equilibrium structures of the neutral and ionic species along with the vibrational normal coordinates. The equilibrium bond lengths of the neutral ground state species and those of the cations in their D_0 and D_1 states are collected in the ESI.†

The D_0 structure of the lactam tautomer was determined for all the species while the D_1 structure of the lactim tautomer was obtained for the parent compound and for 3-Cl, 5-Cl and 6-Cl derivatives but the calculations did not converge for 4-Cl. In addition, for 2HP (lactim tautomer of the parent compound) the vibrational frequency calculations of D_1 displayed unrealistically large values, possibly related to the presence of a quasi-degeneracy with a second excited state. Therefore the vibronic structure of the $S_0 \rightarrow D_1$ transition for 2HP could not be determined.

The TD-DFT wavefunction of the D_1 state (reported in Table 4 for all the species) is in all cases dominated by the same single electronic excitation whose graphical representation is shown in Fig. 14 for 3Cl-2HP and 3Cl-2PO, as a representative example, and in the ESI† for the remaining compounds. From the wavefunction we see that the D_1 state corresponds to ionization of a σ orbital with a large non-bonding character on the nitrogen (for lactim derivatives) or on the oxygen (for lactam derivatives). Conversely, the ground state of the cationic species, in all cases, corresponds to ionization of the HOMO which is a π orbital (see Fig. 11–13).

4.7 The first ionization or $S_0 \rightarrow D_0$ transition

The neutral-to-cation computed geometry changes, reflect both the nature of the orbital from which the electron has been ejected and also govern the vibronic structure in the photoelectron spectrum. The HOMO orbital displays a similar shape for both lactim and lactam tautomers, as shown in Fig. 11–13. Because of the π nature of the orbital, the bond lengths between heavy atoms change remarkably upon ionization and in similar directions for lactims and lactams (see Fig. 15). Because the HOMO orbital is antibonding with respect to the carbonyl bond for both tautomers, the C–O bond shortens in the cationic state for all the species considered. Similarly, a bond length shortening occurs for the C–Cl bond of substituted derivatives. Other bond length changes can generally be accounted for by inspecting the bonding or antibonding character of the HOMO on specific bonds: those bonds where the orbital is bonding experience an elongation in D_0 and the opposite occurs where the HOMO is antibonding.

These geometry changes are reflected in a marked but not too extended vibronic structure, determined by the activity of in-plane vibrations, most of which are associated with relatively high frequencies. This can be appreciated by inspecting the

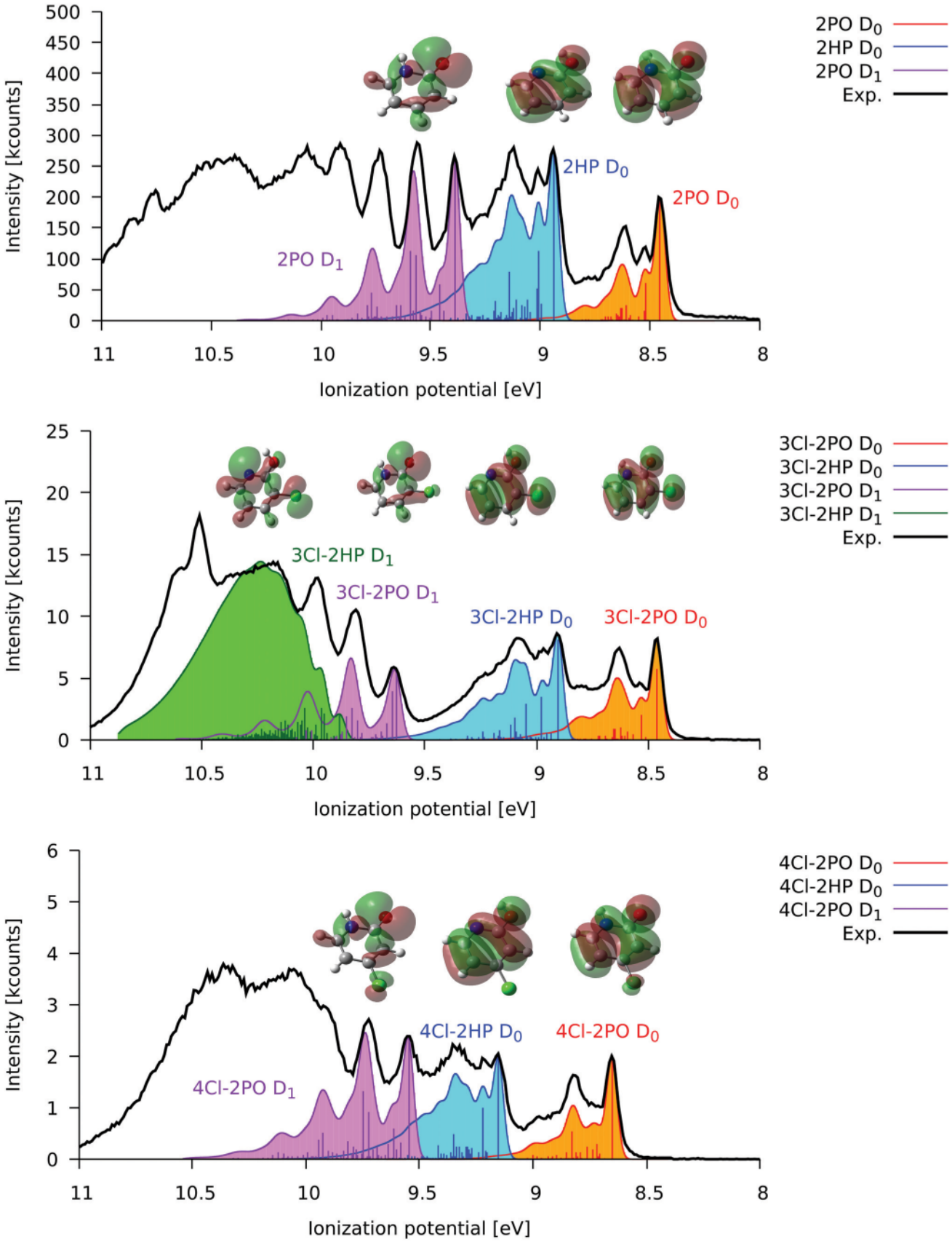

Fig. 11 Experimental valence band photoemission spectrum of 2HP/2PO, 3Cl-2HP/3Cl-2PO and 4Cl-2HP/4Cl-2PO in the 8–11 eV region compared to the simulated vibrational resolved bands, and S_0 molecular orbitals involved in ionization.

Table 4 TD-B3LYP/aug-cc-pVTZ wavefunction of the D_1 state. Orbital labels refer to the neutral HOMO (H) and LUMO (H−1) levels

2HP	1.00 $[(H-1)\beta \rightarrow (H)\beta]$	2PO	0.99 $[(H-1)\beta \rightarrow (H)\beta]$
3Cl-2HP	1.00 $[(H-1)\beta \rightarrow (H)\beta]$	3Cl-2PO	0.98 $[(H-1)\beta \rightarrow (H)\beta]$
		4Cl-2PO	0.97 $[(H-1)\beta \rightarrow (H)\beta]$
5Cl-2HP	1.00 $[(H-1)\beta \rightarrow (H)\beta]$	5Cl-2PO	0.98 $[(H-1)\beta \rightarrow (H)\beta]$
6Cl-2HP	1.00 $[(H-1)\beta \rightarrow (H)\beta]$	6Cl-2PO	0.98 $[(H-1)\beta \rightarrow (H)\beta]$

magnitude of computed Huang–Rhys factors in Table 5. Interestingly, the largest Huang–Rhys factors are computed for a mode around 550 cm^{-1} and for a number of modes with frequencies generally above 1000 cm^{-1}. A plot of the most active vibrational modes (Huang–Rhys factor greater than 0.1) is collected in the ESI.† The modes active in the $S_0 \rightarrow D_0$ transition are similar for lactims and lactams, on account of the similar nature of the depleted orbital in both tautomers.

The simulated spectra of the $S_0 \rightarrow D_0$ transition, shown in Fig. 11–13 in red/orange-shaded curves for the lactam species and in blue/cyan-shaded curves for the lactim species, were rigidly shifted to superimpose the first simulated band with the first observed band of the transition. The identification of the experimental origin band of the $S_0 \rightarrow D_0$ transition is straightforward for the parent compound and for 3-Cl and 4-Cl derivatives, having non negligible populations of both tautomers, while it is more difficult to identify for 5Cl-2PO and 6Cl-2PO. However, our calculations indicate that also for the chlorinated species the first ionization energy of lactam should be smaller than that of the lactim tautomer by about 0.4–0.5 eV. In this view the small features around 8.5 eV in Fig. 12 and 13 can be assigned to the $S_0 \rightarrow D_0$ transition of 5Cl-2PO and 6Cl-2PO.

For all the species, the simulated spectra are dominated by a large intensity of the vibronic band and the intensity of the vibronic progressions fades away about 3000 cm^{-1} from the origin, owing to the moderate values of the Huang–Rhys factors which imply very small intensity for overtones and combination bands. Furthermore, the similar orbital nature of the photoionization determines an overall similar progression of the $S_0 \rightarrow D_0$ transition for both tautomers. The good agreement between predicted and observed vibronic progressions of the $S_0 \rightarrow D_0$ transition leaves no doubt about the correct identification of the 0_0^0 transitions, whose energies are summarized in Table 6.

The simulated $S_0 \rightarrow D_0$ spectra for the two tautomers of the parent compound are also in excellent agreement with the high resolution spectrum[10] (see Fig. 16) and support the assignment of most observed bands to fundamentals. However, in contrast with the tentative assignment proposed by Poully *et al.*[10] it is clear that the band observed at 9.372 eV cannot be assigned to the 1_0^1 vibronic band belonging to the $S_0 \rightarrow D_0$ transition of 2HP. We therefore propose that the origin of the $S_0 \rightarrow D_1$ transition of 2PO, previously assigned to the 9.54 eV band, is instead the 9.372 eV band (corresponding to the 9.39 eV band observed in our spectrum) and we support this assignment with the simulations of the $S_0 \rightarrow D_1$ transition described in Section 4.10.

4.8 Effect of chlorine on ionization potentials

Although the computed adiabatic ionization potentials collected in Table 6 are lower than the observed ones (by about 0.16/0.23 eV for lactams D_0/D_1 and 0.20/0.36 eV for lactims D_0/D_1), the overall trend is in reasonable agreement, as well as the shifts between chlorinated and parent compounds.

Chlorination results in an increase (7–235 meV) of the ionization potential in all cases except for 3Cl-2HP D_0 (−35 meV) and 5Cl-2HP D_0 (−110 meV) and is generally well reproduced by the calculations. The IP changes can be rationalized by considering that inductive and mesomeric (or resonance) effects act in opposite directions for chlorine. Although Cl, an electron-withdrawing group, decreases the electron density on the aromatic ring by a negative inductive effect, it also delocalizes nonbonding electrons onto the phenyl ring by resonance, thereby increasing its electron

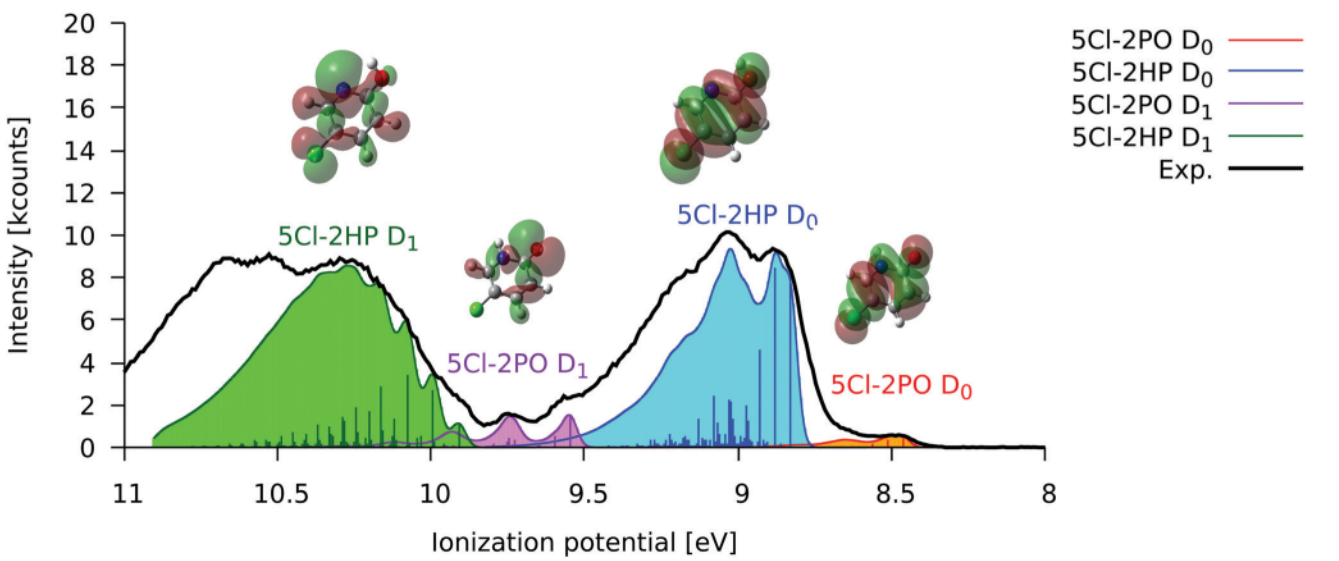

Fig. 12 Experimental valence band photoemission spectrum of 5Cl-2HP/5Cl-2PO in the 8–11 eV region compared to the simulated vibrational resolved bands, and S_0 molecular orbitals involved in ionization.

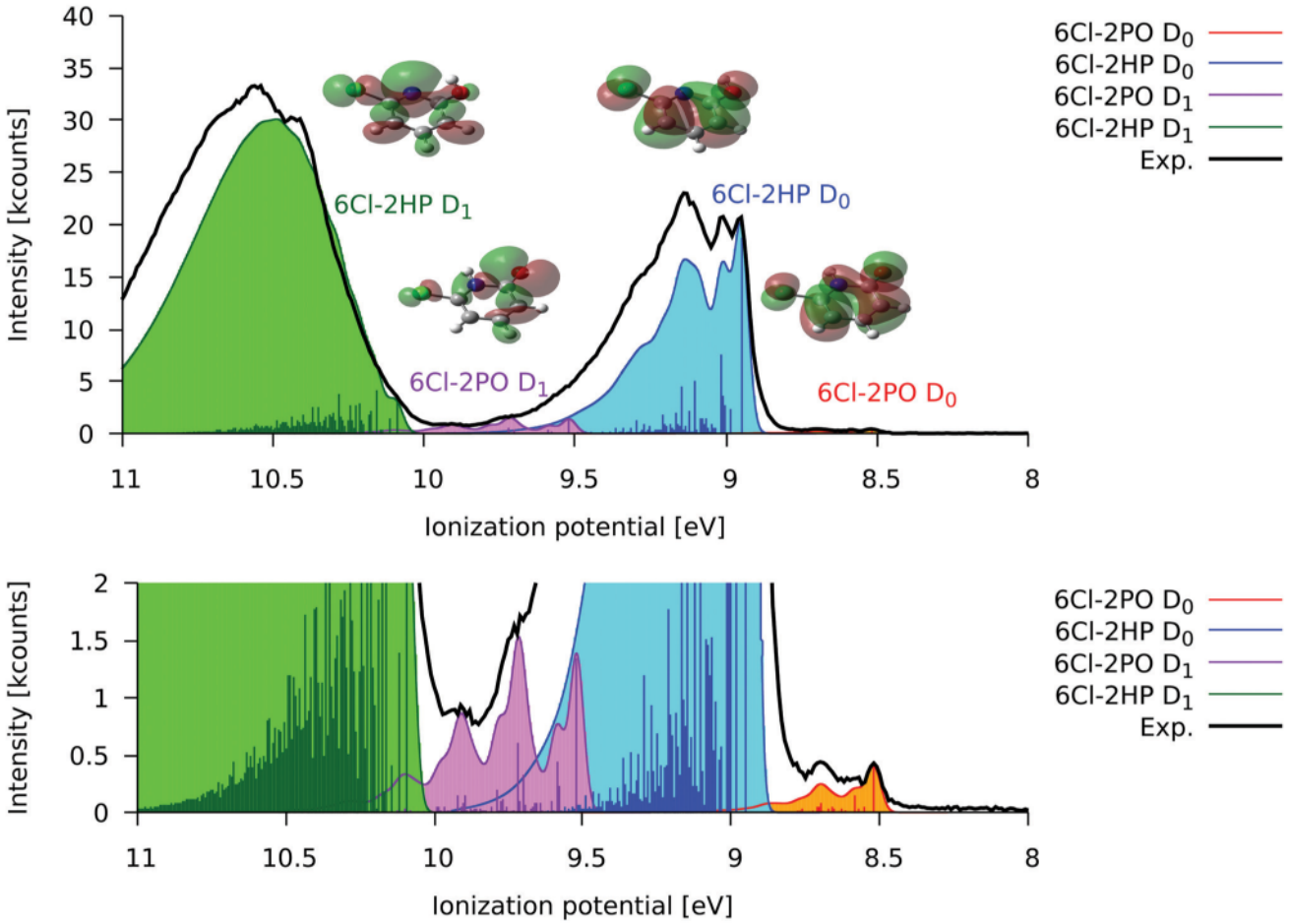

Fig. 13 Experimental valence band photoemission spectrum of 6Cl-2HP/6Cl-2PO in the 8–11 eV region compared to the simulated vibrational resolved bands, and S_0 molecular orbitals involved in ionization.

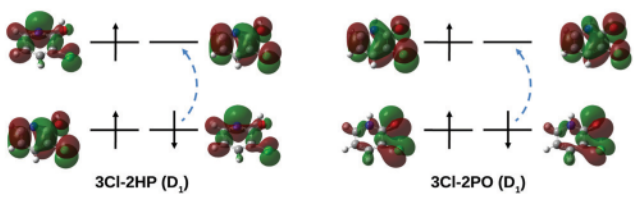

Fig. 14 Frontier molecular orbitals of 3-chloro-2-hydroxypyridine and 3-chloro-2-pyridone at D_1 geometry. Dashed arrows indicate the excitation dominating the D_1 state.

density. As a consequence, the inductive effect will lower the energy of occupied orbitals while the mesomeric effect will tend to increase it. Thus, the changes upon chlorination are expected to be different for the IPs associated with the generation of D_0 or D_1 cationic states. More specifically, when ionization occurs from the HOMO orbital, which is a π orbital, the mesomeric effect is expected to dominate, while the inductive effect is expected to dominate for ionization from the HOMO−1 orbital, which is a σ orbital. As for the mesomeric effect, resulting from π-electron delocalization, one should also consider that Cl is an *ortho–para* director.

Focusing on D_0, the comparison within the lactam forms shows that the shifts of 3Cl-2PO D_0 (7 meV) and 5Cl-2PO D_0 (10 meV) are significantly smaller than those of 4Cl-2PO (198 meV) and 6Cl-2PO (65 meV). Similarly, 3Cl-2HP and 5Cl-2HP display a smaller IP than 4Cl-2HP and 6Cl-2HP. Thus, the 4Cl/6Cl and 3Cl/5Cl pairs have a different behaviour that can be related to the fact that the first are in *para–ortho* to NH or N, while the second are in *ortho–para* to CO or OH. A more efficient mesomeric effect will tend to compensate the inductive effect and reduce the IP. This occurs for 3-Cl and 5-Cl compounds showing always a smaller IP than 4-Cl and 6-Cl compounds, which indicates a more efficient mesomeric effect for the *ortho* or *para* positions with respect to CO or OH.

Moving to D_1, in this case the IPs of all chlorine derivatives are larger than that of the parent molecule, on account of the inductive effect which dominates for the σ orbital.

4.9 Tautomeric equilibrium in the D_0 state

The availability of the adiabatic ionization potentials (corresponding to the 0_0^0 $S_0 \rightarrow D_0$ transition) for both tautomers, enables us to determine the relative energy of the tautomers in their cationic ground state as shown, schematically in Fig. 17. Referring to this figure, the energy difference between the two tautomers in their cationic state can be calculated as:

$$\Delta E(D_0) = (IP_{lactam} - IP_{lactim}) + \Delta E(S_0) \qquad (5)$$

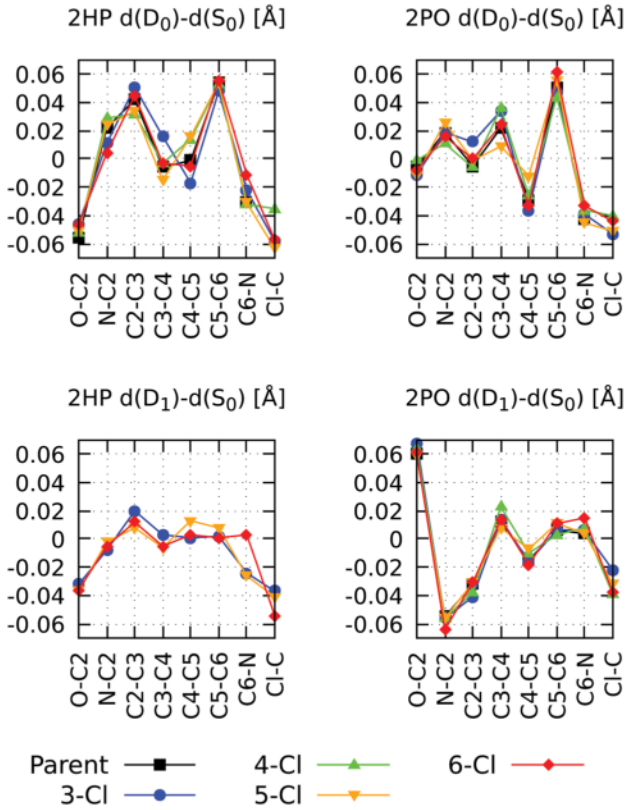

Fig. 15 Changes of the bond distances induced by ionization in parent and chlorinated 2-hydroxypyridine (left) and 2-pyridone (right): (top) differences between bond distances in D_0 and in S_0; (bottom) differences between bond distances in D_1 and in S_1.

using the $\Delta E(S_0)$ values reported in Table 3 and the adiabatic IP(D_0) values collected in Table 6, respectively. The experimental results, compared to the theoretical ones in Table 7, indicate that, in contrast with the preference for the lactim tautomer in the neutral species, the lactam tautomer largely dominates the cationic state.

4.10 The second ionization or $S_0 \rightarrow D_1$ transition

Inspection of the optimized geometries (given in the ESI†) shows that ejection of the electron from the σ orbital to generate the cation in its excited state D_1 causes not only bond length changes but also remarkable ring deformations. This is especially true for the lactim derivatives (∠CNC increases by about 13°) since the σ orbital displays a large non-bonding contribution on the nitrogen. The relevant geometry changes are reflected in generally larger Huang–Rhys factors computed for the $S_0 \rightarrow D_1$ transition (Table 8) compared to those of the $S_0 \rightarrow D_0$ transition. Because the depleted σ orbital is not identical for lactam and lactim derivatives, the $S_0 \rightarrow D_1$ geometry change is also rather different for the two tautomers (see for example Fig. 15 as regard bond length changes) and the same is true for the Huang–Rhys factors (see Table 8) that are generally larger for lactims compared to lactam derivatives.

The largest computed Huang–Rhys factors (*i.e.* greater than 0.1) for the $S_0 \rightarrow D_1$ transition of lactam tautomers are

Table 5 B3LYP/aug-cc-pVTZ vibrational wavenumbers (ν_k [cm^{-1}]) and Huang–Rhys factors (S_k) for the $S_0 \rightarrow D_0$ transition of parent and chlorinated 2-hydroxypyridine and 2-pyridone

2HP		3Cl-2HP		4Cl-2HP		5Cl-2HP		6Cl-2HP	
ν_k	S_k	ν_k	S_k	ν_k	S_k	ν_k	S_k	ν_k	S_k
427	0.10	249	0.06	396	0.07	270	0.02	268	0.13
545	0.41	392	0.07	458	0.09	393	1.09	413	0.15
610	0.19	498	0.02	547	0.51	624	0.04	474	0.19
851	0.05	575	0.43	702	0.07	683	0.05	545	0.40
984	0.12	684	0.03	921	0.11	857	0.03	690	0.03
1003	0.01	884	0.02	986	0.05	1000	0.01	929	0.08
1163	0.09	1012	0.05	1053	0.09	1107	0.16	983	0.05
1176	0.08	1088	0.05	1119	0.03	1147	0.26	1106	0.01
1366	0.02	1154	0.36	1144	0.12	1181	0.05	1110	0.04
1384	0.12	1284	0.02	1274	0.07	1308	0.07	1172	0.02
1486	0.08	1368	0.05	1367	0.01	1363	0.02	1218	0.27
1546	0.02	1396	0.01	1386	0.12	1412	0.02	1373	0.12
1603	0.28	1463	0.02	1477	0.12	1450	0.07	1472	0.03
		1505	0.08	1601	0.24	1504	0.01	1572	0.24
		1557	0.23			1525	0.01		
		1567	0.09			1627	0.29		

2PO		3Cl-2PO		4Cl-2PO		5Cl-2PO		6Cl-2PO	
ν_k	S_k	ν_k	S_k	ν_k	S_k	ν_k	S_k	ν_k	S_k
452	0.01	248	0.01	258	0.01	273	0.09	260	0.12
539	0.30	392	0.04	407	0.05	388	0.75	411	0.08
604	0.08	567	0.36	478	0.03	617	0.03	536	0.37
771	0.04	854	0.07	538	0.17	765	0.05	684	0.01
997	0.01	1047	0.01	698	0.10	765	0.05	853	0.09
1026	0.01	1066	0.13	852	0.12	1105	0.08	1119	0.11
1091	0.01	1169	0.02	1097	0.08	1137	0.09	1174	0.02
1178	0.01	1184	0.01	1119	0.01	1226	0.06	1223	0.07
1229	0.04	1263	0.06	1226	0.03	1252	0.05	1363	0.03
1256	0.12	1302	0.18	1251	0.08	1328	0.12	1430	0.19
1386	0.10	1461	0.02	1305	0.01	1452	0.01	1472	0.11
1474	0.10	1490	0.16	1403	0.29	1492	0.08	1532	0.11
1487	0.03	1569	0.16	1478	0.01	1522	0.02	1559	0.01
1560	0.05	1598	0.02	1594	0.08	1600	0.11		
1610	0.06					1645	0.01		

distributed over a restricted number of vibrational modes. Thus, there are generally one or two active modes below 600 cm^{-1} and two or three strongly active modes in the 1400–1600 cm^{-1} region (graphical representation available in the ESI†). Very little vibronic activity is predicted for modes in between these two regions. As a result, the predicted vibronic progression is characterized by a strong and sharp band located at about 1400–1600 cm^{-1} from the origin followed by its overtones. This peculiar vibronic structure perfectly fits the sequence of bands observed starting at 9.39 eV for the parent compound (9.372 eV in ref. 10, see also the violet simulated spectrum in Fig. 16) at 9.625 eV for 3-Cl and at 9.548 eV for 4-Cl derivatives, namely just above the end of the $S_0 \rightarrow D_0$ progression of the lactim tautomer. Therefore we assign these strongly characterizing groups of bands to the $S_0 \rightarrow D_1$ transition of lactam tautomers.

The computed Huang–Rhys factors for the $S_0 \rightarrow D_1$ transition of the lactim tautomers follow a different trend: a large number of low frequency modes (below 1000 cm^{-1}) display very large values while there are just few additional modes above 1200 cm^{-1} with comparably much lower activity (graphical representation available in the ESI†). This pattern results from the large ring

Table 6 Observed and calculated (B3LYP/aug-cc-pVTZ) adiabatic ionization potentials (0_0^0 transition), in eV, related to the D_0, and D_1 states of parent and chlorinated 2-hydroxypyridine and 2-pyridone. Shifts due to chlorination, with respect to the parent compound, are reported in parenthesis

	Obs.	Calc.	c.–o.
2PO D_0	8.455	8.324	−0.131
3Cl-2PO D_0	8.462 (0.007)	8.278 (−0.046)	−0.184
4Cl-2PO D_0	8.653 (0.198)	8.511 (0.187)	−0.142
5Cl-2PO D_0	8.465 (0.010)	8.293 (−0.031)	−0.172
6Cl-2PO D_0	8.520 (0.065)	8.374 (0.050)	−0.146
2HP D_0	8.940	8.764	−0.176
3Cl-2HP D_0	8.905 (−0.035)	8.685 (−0.079)	−0.220
4Cl-2HP D_0	9.153 (0.213)	8.983 (0.219)	−0.170
5Cl-2HP D_0	8.830 (−0.110)	8.602 (−0.162)	−0.228
6Cl-2HP D_0	8.950 (0.010)	8.736 (−0.028)	−0.214
2PO D_1	9.390	9.169	−0.221
3Cl-2PO D_1	9.625 (0.235)	9.352 (0.183)	−0.273
4Cl-2PO D_1	9.548 (0.158)	9.337 (0.168)	−0.211
5Cl-2PO D_1	9.548 (0.158)	9.296 (0.127)	−0.252
6Cl-2PO D_1	9.520 (0.130)	9.309 (0.140)	−0.211
2HP D_1		9.340	−0.176
3Cl-2HP D_1	9.880	9.547 (0.207)	−0.333
5Cl-2HP D_1	9.910	9.566 (0.127)	−0.344
6Cl-2HP D_1	10.090	9.692 (0.352)	−0.398

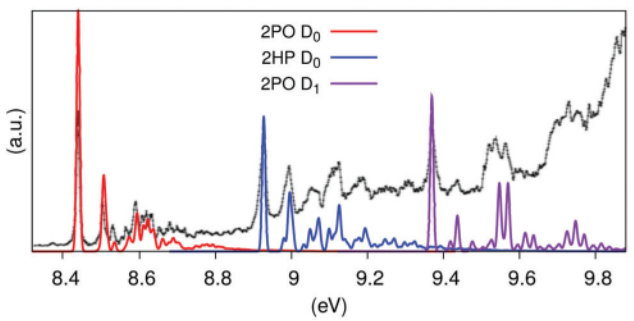

Fig. 16 The simulated photoelectron spectra of 2-pyridone D_0 (red trace), 2-hydroxypyridine D_0 (blue trace) and 2-pyridone D_1 (violet trace) are superimposed to the high resolution spectrum adapted from Poully *et al.*[10]

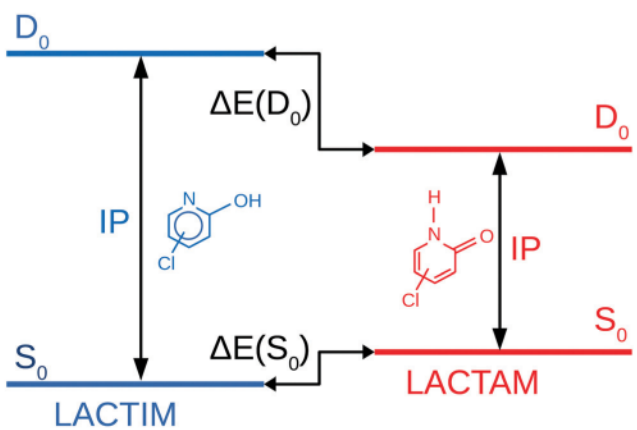

Fig. 17 Schematic representation of the relative position of 2-hydroxypyridine and 2-pyridone compounds in the neutral (S_0) and cationic (D_0) ground states.

Table 7 Experimental and theoretical relative energy values of parent and chlorinated 2-hydroxypyridine with respect to 2-pyridone in the D_0 state: $\Delta E = E_{lactam} - E_{lactim}$ [kJ mol^{-1}]

	Parent	3-Cl	4-Cl	5-Cl	6-Cl
Exp.	−46.8	−41.6	−45.9	−26.7	−30.0
Calc.	−44.8	−42.3	−48.5	−24.9	−24.7

Table 8 B3LYP/aug-cc-pVTZ vibrational wavenumbers (ν_k [cm^{-1}]) and Huang–Rhys factors (S_k) for the $S_0 \rightarrow D_1$ transition of parent and chlorinated 2-hydroxypyridine and 2-pyridone

3Cl-2HP		5Cl-2HP		6Cl-2HP	
ν_k	S_k	ν_k	S_k	ν_k	S_k
238	0.16	262	0.02	208	0.44
486	0.29	388	0.17	415	0.07
582	0.98	423	0.06	428	0.13
694	1.21	648	0.25	553	1.33
856	0.57	678	2.55	703	0.66
1058	0.33	991	0.51	942	0.40
1086	0.06	1108	0.04	980	0.92
1123	0.07	1138	0.01	1076	0.07
1214	0.04	1162	0.03	1136	0.02
1286	0.14	1220	0.01	1166	0.05
1440	0.02	1292	0.21	1200	0.02
1510	0.01	1363	0.04	1245	0.13
1543	0.25	1548	0.05	1369	0.09
1612	0.13	1648	0.37	1424	0.16
				1554	0.19
				1623	0.16

2PO		3Cl-2PO		4Cl-2PO		5Cl-2PO		6Cl-2PO	
ν_k	S_k	ν_k	S_k	ν_k	S_k	ν_k	S_k	ν_k	S_k
395	0.07	179	0.72	256	0.13	259	0.01	255	0.01
542	0.23	391	0.01	408	0.08	390	0.36	456	0.17
859	0.06	474	0.01	544	0.26	636	0.01	546	0.33
1198	0.04	572	0.13	723	0.12	673	0.02	692	0.07
1248	0.01	708	0.05	1107	0.11	861	0.09	1147	0.06
1273	0.06	879	0.01	1262	0.08	1123	0.03	1198	0.03
1395	0.04	1089	0.01	1348	0.02	1159	0.02	1255	0.03
1435	0.41	1231	0.01	1424	0.39	1237	0.01	1372	0.02
1520	0.06	1270	0.10	1486	0.02	1279	0.08	1420	0.05
1616	0.43	1332	0.05	1601	0.56	1344	0.02	1444	0.25
		1445	0.30			1439	0.24	1525	0.07
		1463	0.01			1455	0.09	1609	0.45
		1523	0.04			1522	0.08	1625	0.24
		1629	0.48			1615	0.34		
		1646	0.30			1648	0.18		

deformation around the nitrogen atom and is reflected in an extended vibronic structure broadened by the activity of low frequency modes and by the large number of overtones and combination bands. Interestingly, such extended vibronic structure fits nicely with the extended structure observed in the highest energy region of all the experimental spectra shown in Fig. 11–13.

Finally, as regards 2HP, we can attempt a comparison with the parent aromatic compound, pyridine. For this molecule Trofimov *et al.*,[38] applying high-level computational methods (equation-of-motion coupled-cluster with single, double, and triple excitations and the complete basis set extrapolation technique), assigned the 9.64 and 9.85 eV features to the ionization of the σ_N and π orbitals, respectively. This means that due to the introduction of the hydroxyl group, the ionization energy of the

highest occupied π orbital changes from 9.85 to 8.94 eV, with a downshift of −0.91 eV, in agreement with the expected mesomer effect. Although we did not obtain direct information for the $S_0 \rightarrow D_1$ transition, the shape of the spectrum and the data recorded for the chlorinated species suggest that the ionization energy of the σ_N orbital of 2HP is equal to or greater than that of pyridine. Indeed, due to the inductive, charge-withdrawing action of the oxygen atom, an increase of the σ_N orbital binding energy is plausible.

5 Conclusions

We have measured and assigned the valence and core photoemission spectra of the tautomers of 2-hydroxypyridine and four of its chlorinated derivatives. The ionization potentials of C(1s), N(1s), O(1s) and Cl(2p) are in quite good agreement with theoretical calculations, which overestimate the observed values by 0.1–0.4%. The C(1s) spectra are rather crowded, but starting form the theoretical predictions and applying a number of constraints, we were able to extract values for the ionization potentials of the tautomers in each compound. We have compared the data to a published model of core level shifts in di-substituted benzenes, and found reasonable agreement. The measurement of the intensities of the two peaks observed for both N(1s) and O(1s) allows an independent estimation of the relative populations of the two tautomers present in the gas sample at the experimental temperature. The lactim tautomer is the most stable for all species. With respect to the parent species, chlorination in position 3 and 4 stabilizes the lactam whereas chlorination in position 5 and 6 strongly stabilizes the lactim. This trend is similar to that predicted by the semi-empirical model of Calabrese *et al.*[19]

The rich fine structure in the 8–11 eV region of the valence band photoionization spectra has been assigned on the basis of simulated vibronic structures associated with the first and second ionization of the lactam and lactim species. The study confirms that, for all species, the lowest energy vibronic structure is due to ionization from the HOMO of the lactam, followed by ionization from the HOMO of the lactim. These two vibronic progressions are relatively similar in shape and extension due to the similar orbital nature of the HOMO for both tautomers. The simulations show that ionization to form the cation of the lactam in its lowest excited state (namely ionization from the HOMO−1) leads to a sequence of highly distinctive vibronic bands that are readily assigned to the structure observed just above the first ionization of the lactim, for three of the five species investigated. The identification and assignment of the adiabatic (0_0^0) first ionization energy, combined with the knowledge of the relative energy of tautomers in the neutral ground state S_0, allowed us to derive the relative stability of the tautomers in the cationic ground state D_0 for all the species, thereby showing that the lactam form always dominates.

Overall, the combined experimental and computational investigation provides a detailed view of the tautomeric equilibrium of 2-hydroxypyridine and its four its chlorinated derivatives, encompassing neutral and cationic species.

Conflicts of interest

There are no conflicts to declare.

Acknowledgements

We thank C. Puglia (Uppsala University, Sweden) and the Carl Tygger Foundation for making available the VG-Scienta SES-200 photoelectron analyser at the Gas Phase beamline, Elettra, Italy. We gratefully acknowledge the financial support of University of Bologna (RFO), MIUR (FABR) and Fondazione Cassa di Risparmio di Bologna. We acknowledge the CINECA award under the ISCRA initiative for the availability of high performance computing resources. We thank Andrea Zanoni for preliminary simulations on 2PO and 2HP. AM and SM acknowledge Elettra Sincrotrone Trieste for providing financial support as Italian Funded Users to attend shifts assigned to the Proposal No. 20170018 at the gas phase beamline. HS acknowledges the TRIL fellowship awarded by the Abdus Salam International Centre for Theoretical Physics (ICTP), Trieste, Italy.

References

1 B. Stanovnik, M. Tišler, A. Katritzky and O. Denisko, in *Advances in Heterocyclic Chemistry*, ed. A. Katritzky, Academic Press, Amsterdam, 2006, ch. 1, vol. 91, pp. 1–134.
2 V. Singh, B. Fedeles and J. Essigmann, *RNA*, 2015, **21**, 1–13.
3 P. Beak, J. F. S. Fry, J. Lee and F. Steele, *J. Am. Chem. Soc.*, 1976, **98**, 171–179.
4 R. Brown, A. Tse and J. Vederas, *J. Am. Chem. Soc.*, 1980, **102**, 1174–1176.
5 L. Lapinski, M. Nowak, J. Fulara, A. Les and L. Adamowicz, *J. Phys. Chem.*, 1992, **96**, 6250–6254.
6 L. Hatherley, R. Brown, P. Godfrey, A. Pierlot, W. Caminati, D. Damiani, S. Melandri and L. Favero, *J. Phys. Chem.*, 1993, **97**, 46–51.
7 H. Abdulla and M. El-Bermani, *Spectrochim. Acta, Part A*, 2001, **57**, 2659–2671.
8 A. Maris, P. Ottaviani and W. Caminati, *Chem. Phys. Lett.*, 2002, **360**, 155–160.
9 L. Forlani, G. Cristoni, C. Boga, P. Todesco, E. D. Vecchio, S. Selva and M. Monari, *ARKIVOC*, 2002, **11**, 198–215.
10 J. Poully, J. Schermann, N. Nieuwjaer, F. Lecomte, G. Grégoire, C. Desfrançois, G. Garcia, L. Nahon, D. Nandi, L. Poisson and M. Hochlaf, *Phys. Chem. Chem. Phys.*, 2010, **12**, 3566–3572.
11 S. Melandri, L. Evangelisti, A. Maris, W. Caminati, B. Giuliano, V. Feyer, K. C. Prince and M. Coreno, *J. Am. Chem. Soc.*, 2010, **132**, 10269.
12 B. Giuliano, V. Feyer, K. Prince, M. Coreno, L. Evangelisti, S. Melandri and W. Caminati, *J. Phys. Chem. A*, 2010, **114**, 12725–12730.
13 A. Michelson, A. Petronico and J. Lee, *J. Org. Chem.*, 2012, **77**, 1623–1631.
14 P. Beak, J. Covington and J. White, *J. Org. Chem.*, 1980, **45**, 1347–1353.
15 M. Piacenza and S. Grimme, *J. Comput. Chem.*, 2004, **25**, 83–98.

16 J. Sonnenberg, K. Wong, G. Voth and H. Schlegel, *J. Chem. Theory Comput.*, 2009, **5**, 949–961.
17 M. B. Messaouda, M. Abderrabba, A. Mahjoub, G. Chambaud and M. Hochlaf, *Comput. Theor. Chem.*, 2012, **990**, 94–99.
18 V. Feyer, O. Plekan, R. Richter, M. Coreno, G. Vall-llosera, K. C. Prince, A. B. Trofimov, I. L. Zaytseva, T. E. Moskovskaya, E. V. Gromov and J. Schirmer, *J. Phys. Chem. A*, 2009, **113**, 5736–5742.
19 C. Calabrese, A. Maris, I. Uriarte, E. Cocinero and S. Melandri, *Chem. – Eur. J.*, 2017, **23**, 3595–3604.
20 K. C. Prince, R. R. Blyth, R. Delaunay, M. Zitnik, J. Krempasky, J. Slezak, R. Camilloni, L. Avaldi, M. Coreno, G. Stefani, C. Furlani, M. de Simone and S. Stranges, *J. Synchrotron Radiat.*, 1998, **5**, 565–568.
21 J. Lüder, M. de Simone, R. Totani, M. Coreno, C. Grazioli, B. Sanyal, O. Eriksson, B. Brena and C. Puglia, *J. Chem. Phys.*, 2015, **142**, 074305.
22 N. Mårtensson, P. Baltzer, P. Brühwiler, J.-O. Forsell, A. Nilsson, A. Stenborg and B. Wannberg, *J. Electron Spectrosc. Relat. Phenom.*, 1994, **70**, 117–128.
23 I. Velchev, W. Hogervorst and W. Ubachs, *J. Phys. B: At., Mol. Opt. Phys.*, 1999, **32**, L511–L516.
24 V. Myrseth, J. Bozekb, E. Kukkc, L. Sæthrea and T. Thomas, *J. Electron Spectrosc. Relat. Phenom.*, 2002, **12**, 57–63.
25 L. Pettersson, J. Nordgren, L. Selander, C. Nordling, K. Siegbahn and H. Ågren, *J. Electron Spectrosc. Relat. Phenom.*, 1982, **27**, 29–37.
26 M. Ehara, J. Hasegawa and H. Nakatsuji, *Theory and Applications of Computational Chemistry. The First Forty Years*, Elsevier, Amsterdam, 2005, ch. 39, pp. 1099–1141.
27 F. Negri and M. Zgierski, *J. Chem. Phys.*, 1992, **97**, 7124–7136.
28 M. Malagoli, V. Coropceanu, D. da Silva Filho and J. Brédas, *J. Chem. Phys.*, 2004, **120**, 7490–7496.
29 F. Duschinsky, *Acta Physicochim. URSS*, 1937, **7**, 551–566.
30 F. Santoro, A. Lami, R. Improta, J. Bloino and V. Barone, *J. Chem. Phys.*, 2008, **128**, 224311.
31 M. Dierksen and S. Grimme, *J. Chem. Phys.*, 2005, **122**, 244101.
32 V. Barone, J. Bloino, M. Biczysko and F. Santoro, *J. Chem. Theory Comput.*, 2009, **5**, 540–554.
33 S. Lunell, M. P. Keane and S. Svensson, *J. Chem. Phys.*, 1989, **90**, 4341–4350.
34 V. Myrseth, K. Børve and T. Thomas, *J. Org. Chem.*, 2007, **72**, 5715–5723.
35 T. X. Carroll, T. D. Thomas, L. J. Sæthre and K. J. Børve, *J. Phys. Chem. A*, 2009, **113**, 3481–3490.
36 A. Hitchcock, M. Pocock, C. Brion, M. Banna, D. Frost, C. McDowell and B. Wallbank, *J. Electron Spectrosc. Relat. Phenom.*, 1978, **13**, 345–360.
37 M. C. Castrovilli, P. Bolognesi, E. Bodo, G. Mattioli, A. Cartoni and L. Avaldi, *Phys. Chem. Chem. Phys.*, 2018, **20**, 6657–6667.
38 A. B. Trofimov, J. Schirmer, V. B. Kobychev, A. W. Potts, D. M. P. Holland and L. Karlsson, *J. Phys. B: At., Mol. Opt. Phys.*, 2005, **39**, 305–329.